Supplementary Material: A Riemannian Approach for Spatiotemporal Analysis and Generation of 4D Tree-shaped Structures

Tahmina Khanam[1], Hamid Laga[1], Mohammed Bennamoun[2], Guanjin Wang[1], Ferdous Sohel[1], Farid Boussaid[2], Guan Wang[3], and Anuj Srivastava[4]

[1] Murdoch University, WA, Australia
34719017@student.murdoch.edu.au, {H.Laga, Guanjin.Wang,F.Sohel}@murdoch.edu.au
[2] University of Western Australia, WA, Australia
{mohammed.bennamoun, farid.boussaid}@uwa.edu.au
[3] Yangtze Delta Region Institute (Huzhou), University of Electronic Science and Technology of China, China, wangguan12621@gmail.com
[4] Florida State University, USA, anuj@stat.fsu.edu

Abstract. This supplementary material provides additional details and results that could not fit in the main manuscript. Sec. 1 describes in detail the 4D dataset we used throughout all our experiments. Sec. 2 provides the detailed spatial registration algorithm used to compute branchwise correspondences between 3D trees belonging to the same 4D tree and across 4D trees. Sec. 3 analyzes the computation time of each component of the proposed framework. Finally, Sec. 4 provides additional results to demonstrate the effectiveness of the proposed framework.

1 The Pheno4D dataset

Throughout the paper, we used the Pheno4D dataset [3], which contains 4D models of seven tomato and seven maize plants captured at different points in time during their growth season. All the models were captured in the form of 3D point clouds and are spatially unregistered; see Fig. 1-(top row) for an example of a growing tomato plant.

The 4D maize plants have been captured at the same points in time. The tomato plants, on the other hand, have been captured at different intervals. In both cases, the plants exhibit significant variability in their growth rates since plants, even if they have been grown under the same conditions, grow at different rates. Thus, all the 4D plants are neither spatially nor temporally registered.

Before using this data in the proposed framework, we first extract, from the 3D point clouds, their 3D skeletal structures using the method proposed in [2]; see the top row of each example in Fig. 1, and organize the skeleton into layers of branches; see the bottom row of each example in Fig. 1.

2 Detailed spatial registration algorithm

Since every 4D tree shape is composed of a sequence of 3D trees, we first spatially register the 3D shapes. First, since two 3D trees can have different numbers of branches, we add null branches so that the two 3D trees have the same number of branches. Algorithm 1 describes the process of putting in correspondence the 3D tree shapes within each 4D sequence. In this algorithm, the function $\text{apply}(\alpha(j), O, \boldsymbol{\gamma}, \boldsymbol{\sigma})$ refers to the process of applying the rotation O, diffeomorphism $\boldsymbol{\gamma}$, and permutations $\boldsymbol{\sigma}$ to the 3D tree shape $\alpha(j)$. We refer to this phase of the spatial registration as *within 4D sequence registration*. Following that, we register every 3D sample across 4D shapes as described in **??** in the main manuscript and we refer to that phase as cross-sequence registration.

In more detail, assume that we have two 3D trees $\alpha(j)$ and $\alpha(j+1)$. We aim to find a rotation O^*, a reparameterization $\boldsymbol{\gamma}^*$ of branches, and a permutation $\boldsymbol{\sigma}^*$ of the order of branches that minimize the distance between $\alpha(j)$ and $\alpha(j+1)$ as defined in **??** and as of **??** in the main manuscript, where Q_1 is equivalent to $\alpha(j)$ and Q_2 is equivalent to $\alpha(j+1)$.

The first term of **??** in the main manuscript measures the distance between two main branches, which is independent of the other two terms. So, we first optimize that first term and get the optimal rotation O^* and reparameterization $\boldsymbol{\gamma}^{0*}$ that elastically aligns the main branch of $\alpha(j+1)$ onto the main branch of $\alpha(j)$. we solve this problem of finding the optimal rotation O^* and reparameterization $\boldsymbol{\gamma}^{0*}$ using dynamic programming introduced as in [4]. Then, we solve the problem of finding which side branch of $\alpha(j+1)$ corresponds to which side branch of $\alpha(j)$ by solving the other two terms of **??** in the main manuscript, as a linear assignment problem. let n_1 be the number of side branches of the main branch of $\alpha(j)$ and n_2 the number of side branches of the main branch of $\alpha(j+1)$. We build a pairwise distance matrix E of size $n_1 \times n_2$ as follows:

$$E_{ij} = \lambda_s \inf_{O,\boldsymbol{\gamma}} \|q_1^i - O(q_2^j, \boldsymbol{\gamma})\|^2 + \lambda_p \left(s_1^i - s_2^j\right)^2, \tag{1}$$

where, q_1, q_2 denote the side branches and s_1 and s_2 are the bifurcation points (connecting points) of those side branches to their parent branches of $\alpha(j)$ and $\alpha(j+1)$, respectively.

When we generate the matrix, we find the optimal O^* and $\boldsymbol{\gamma}^*$ for each pair of branches using the same approach of dynamic programming introduced in [4]. Then, we apply the Hungarian Algorithm to the matrix E to find out the optimal matching $\boldsymbol{\sigma}^*$ between the side branches. At each layer of the trees, and for each branch, we build this matrix and recursively solve all from the highest layer to the main branch.

3 Computation time

The framework proposed in this paper was implemented using MATLAB(2022) running on a CPU with 3.2 GHz Intel Core i7 processor and 16 GB of RAM.

Algorithm 1 Registration within 4D tree sequences

Input and Definition:

- 4D tree shapes, $\alpha_1, \alpha_2, \ldots \alpha_n$ and n = number of 4D trees
- $n_$samples: the number of 3D samples within each 4D tree. Note that different 4D tree shapes have different $n_$samples.

Procedure:

for $i \leftarrow 1$ to n **do**
  $n_$samples $\leftarrow size(\alpha_i)$
  for $j \leftarrow 1$ to $n_$samples **do**
    find: $(O^*, \boldsymbol{\gamma}^*, \boldsymbol{\sigma}^*) = \underset{O,\boldsymbol{\gamma},\boldsymbol{\sigma}}{\operatorname{argmin}} d_{\mathcal{C}_Q}(\alpha_i(j), \alpha_i(j+1))$ [**??** in main manuscript]
    update: $\tilde{\alpha}_i(j+1) = \text{apply}(\alpha_i(j+1), O^*, \boldsymbol{\gamma}^*, \boldsymbol{\sigma}^*)$
  end for
  output spatially registered 4D tree: $\tilde{\alpha}_i$
end for

Spatial registration		Temporal registration			
SRVF space		SRVF space		PCA space	
Tomato	Maize	Tomato	Maize	Tomato	Maize
235s	17s	1,786s	176s	0.037s	0.006s

Table 1: Maximum computational time for the spatiotemporal registration (in seconds).

Tabs. 1 and 2 provide a detailed breakdown of the computation time of the different components of the proposed framework. The maximum time required for the spatial registration of two 4D maize plants was around 17 seconds and was 235 seconds for the tomato plants. From Tab. 1, we can see that the computation time required for the spatial registration increases with the complexity of the branching structure of the tree-shaped 3D objects. For instance, the maize plants have only two levels of layers and the computation time for putting in correspondence two such 3D objects is 17s on average. The tomato plants, on the other hand, which can have up to four layers, require, on average, 235 seconds.

One important contribution of this paper is the mapping of 4D tree-shaped structures to a low-dimensional PCA space where 4D tree-shaped structures become trajectories in a low-dimensional space. This resulted in a significant improvement in the computation time of the temporal registration: in the original SRVF space, the temporal registration takes on average 176s for the maize plant and 1,786s for the tomato plant. In the proposed PCA space, this computation time is significantly reduced to 0.006 seconds for the maize plant and 0.037 seconds for the tomato plant. The gain in computation time comes without sacrifying the quality and accuracy of the temporal registration.

Geodesic		Mean		Modes of variation		Synthesis	
Tomato	Maize	Tomato	Maize	Tomato	Maize	Tomato	Maize
0.025s	0.007s	0.0006s	0.0004s	0.002s	0.001s	0.001s	0.0006s

Table 2: Maximum computation time (in seconds) for computing 4D geodesics between two 4D tree-shaped structures, 4D statistics (mean and modes of variation), and generating (synthesizing) one 4D tree-shaped structure..

Once the spatiotemporal registration is performed, the subsequent steps, *i.e.,* computing 4D geodesics, means and modes of variation, and generating new 4D tree-shaped structures is very fast, in the order of milliseconds as shown in Tab. 2.

4 Additional results

In this section, we provide more results and analysis that could not fit within the main manuscript. In what follows, Sec. 4.1 discusses the spatiotemporal registration. Sec. 4.2 presents additional results about geodesics between 4D tree-shaped structures. Sec. 4.3 provides additional results on summary statistics while Sec. 4.4 provides more examples of randomly generated 4D tree-shaped structures.

4.1 Spatiotemporal Registration

Spatial registration. Figs. 2 and 24 show two examples of the spatial registration of the 3D trees within two 4D tomato plants, hereinafter referred to as the source and target plants. In the figures, we show the source and target 4D plants before and after spatial registration. Here, for clarity purposes, we only show the branch-wise correspondences up to the 2^{nd} layer. Fig. 3 provides a zoom-in on the highlighted 3D trees while Fig. 4 shows the computed correspondences at the third level of the tree hierarchy. These figures show that our proposed framework is efficient in finding correct branch-wise correspondences between complex 4D plants.

Fig. 13 provides another example showing the computed spatial registrations within and across a 4D maize plant.

In addition to the performance metrics used in the main manuscript, we also evaluate the quality of the proposed spatial registration and compare it to [2] and [1] using the *the description length* defined as the number of eigenvectors needed to characterize $x\%$ of the variability within the dataset. x is referred to as the cumulative energy. To this end, we take a collection of twenty-eight 3D trees, compute their spatial correspondences using the three methods, and then perform PCA on the aligned dataset. If the spatial correspondences are correct then the number of eigenvectors needed to describe $x\%$ of the variability in the dataset should be small. x is referred to as the cumulative energy while the number of eigenvectors is referred to as the description length. Fig. 5 plots

the cumulative energy vs. the description length before spatial registration and after the spatial registration using our method and the methods of [2] and [1]. As we can see, our method performs slightly better than [2] and [1]. This difference becomes significant for cumulative energies that are below 65%. However, on average, [1] requires 30s, [2] requires 20.1s, while our method requires only 2.3s to register two 3D trees. This shows that the proposed method is significantly faster than [1] and [2] without sacrificing the quality of the registration. In the contrary, our method performs slightly better as shown in Fig. 5.

Temporal registration: In this section, we demonstrate the proposed framework's performance in temporally aligning 4D plants that grow at different rates. Using the datasets described above, we first randomly remove some samples to simulate unsynchronised 4D plants and use these re-sampled 4D sequences to validate our proposed temporal registration tools. Fig. 6 shows an example where the target 4D tree has been temporally warped, using the proposed framework, to temporally align it onto the source 4D tree. To visually evaluate the quality of the proposed temporal alignment, we also show the ground-truth target 4D plant in Fig. 6 along with the temporally registered 4D target plant. From the figure, we can see that, after the temporal registration, the growth rate becomes closer to the ground truth. The supplementary material provides more results of temporal registration of 4D tomato and maize plants.

Fig. 14 shows another example of temporal registration between two 4D maize plants. Further, we add more temporal registration results between 4D tomato plants in Figs. 25 to 27.

Ablation study. The importance of the SRVF representation in spatial registration of 3D tree shapes has already been established in [5]. Thus, in this paper, we only analyze the importance of the SRVF representation in performing temporal registration. To this end, we take a ground truth 4D source plant and generate a target 4D plant by temporally warping the source. Hence, the target becomes non-synchronized with the source. We then register the source and target 4D plants in the spatial domain as well as in the SRVF domain. We can observe in Fig. 7 that in the original space, the temporal registration failed to synchronize the target with the source. Also, we observe a significant shrinkage in the 4D target plant, and thus cannot properly represent the growth of the target plant; see the region highlighted with a green box. We can clearly see incorrect temporal registration results when using the $\mathbb{L}^2$ metric. This is expected since the tree shape space has a non-linear structure. Also, when working in the original space, we observe that branches get disconnected from their parent branch at the bifurcation points; see the red box in Fig. 7. Fig. 7b and Fig. 7c show a zoom-in on the regions highlighted with a red box in Fig. 7.

4.2 Geodesics between 4D Trees

Fig. 8 shows a geodesic path, before spatiotemporal registration, between a source 4D plant (top row) and a target 4D plant (bottom row). The in-between rows correspond to 4D plants sampled at equidistances along the geodesic path

between the source and target. In this example, the target has a different growth rate than the source 4D plant. It also has missing samples. Thus, we interpolate it and sample it at the same time intervals as the source but we do not perform spatiotemporal registration. Consequently, the target follows a different growth pattern than the source. As we can see in this figure, since the two 4D plants are not spatio-temporally registered, the 4D geodesic does not look realistic as the intermediate 4D plants along the geodesic exhibit significant shrinkage. Fig. 9 shows the geodesic between the same 4D plants but after performing spatiotemporal registration using the proposed framework. We can clearly see now that the target 4D plant (last row) is temporally well aligned with the source 4D plant (first row). Also, we can clearly see that the branches of the intermediate plants along the geodesic path (intermediate rows) do not suffer from the shrinkage observed in Fig. 8, prior to the registration.

Fig. 15 and Fig. 16 show another example of geodesics between 4D maize plants before (Fig. 15) and after (Fig. 16) temporal registration. We also computed the geodesic between 4D maize plants by mapping the 3D trees into curve space from their original tree shape space $\mathcal{C}_T$, instead of SRVFT space $\mathcal{C}_Q$. We show this result in Fig. 17 where we can notice a significant noise added in the geodesic path.

4.3 Summary Statistics

We take seven unregistered 4D tomato plants from the Pheno4D dataset and compute their mean and modes of variations using the proposed framework. Fig. 10 shows the seven 4D tomato plants before (Fig. 10a) and after (Fig. 10b) co-registering using the proposed spatiotemporal registration. In the figure, each row corresponds to a 4D plant and the color codes represent the branch-wise correspondences. Before registration, the branch correspondences were not correct. Although the growth rate varies across the 4D plants, and thus the plants are not temporally registered, we have further removed some samples in some of the 4D plants to simulate highly unsynchronized 4D plants. After spatiotemporal co-registration, we can observe that the branches of the 4D plants become in correspondence. Further, all the 4D plants become temporally synchronized with each other irrespective of their growth rates.

Fig. 11 shows the average 4D plant of these seven registered 4D plants computed using the proposed framework. We can see that the mean captures the main characteristics of these seven 4D plants.

In addition to the mean, Fig. 12 shows the principle directions of variation that represent the spatiotemporal shape variability in the seven 4D tomato plants.

We also perform the same task on seven unregistered 4D maize plants (Fig. 18) from Pheno4D. Fig. 19 shows the same 4D plants after their co-registration (spatially and temporally), Fig. 20 shows their computed 4D mean while Figs. 21 and 22 show, respectively, the first and second modes of variation.

4.4 4D Tree-shape Synthesis

In addition to the examples presented in the main manuscript, Fig. 23 shows four randomly synthesized 4D maize plants.

References

1. Chebrolu, N., Magistri, F., Läbe, T., Stachniss, C.: Registration of spatio-temporal point clouds of plants for phenotyping. PloS one **16**(2), e0247243 (2021)
2. Pan, H., Hétroy-Wheeler, F., Charlaix, J., Colliaux, D.: Multi-scale space-time registration of growing plants. In: 2021 International Conference on 3D Vision (3DV). pp. 310–319. IEEE (2021)
3. Schunck, D., Magistri, F., Rosu, R.A., Cornelißen, A., Chebrolu, N., Paulus, S., Léon, J., Behnke, S., Stachniss, C., Kuhlmann, H., et al.: Pheno4d: A spatio-temporal dataset of maize and tomato plant point clouds for phenotyping and advanced plant analysis. Plos one **16**(8), e0256340 (2021)
4. Srivastava, A., Klassen, E., Joshi, S.H., Jermyn, I.H.: Shape analysis of elastic curves in euclidean spaces. IEEE transactions on pattern analysis and machine intelligence **33**(7), 1415–1428 (2010)
5. Wang, G., Laga, H., Srivastava, A.: Elastic shape analysis of tree-like 3d objects using extended srvf representation. IEEE Transactions on Pattern Analysis and Machine Intelligence (2023)

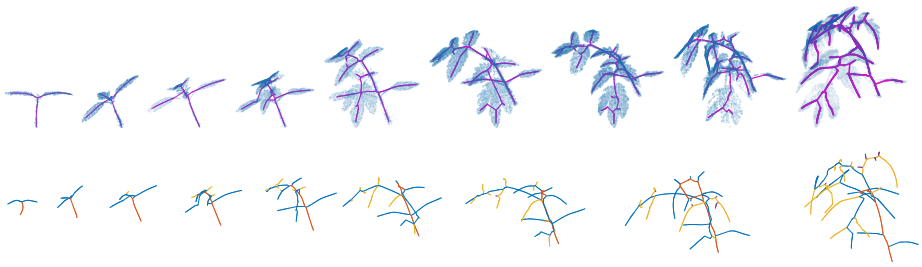

(a) An example of a growing tomato plant.

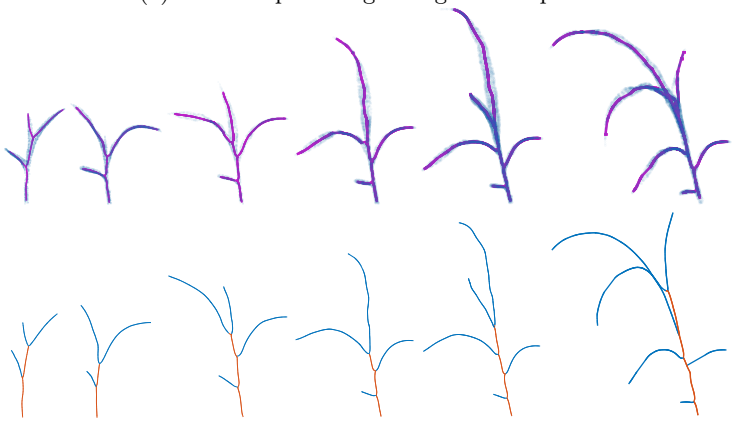

(b) An example of growing maize plant.

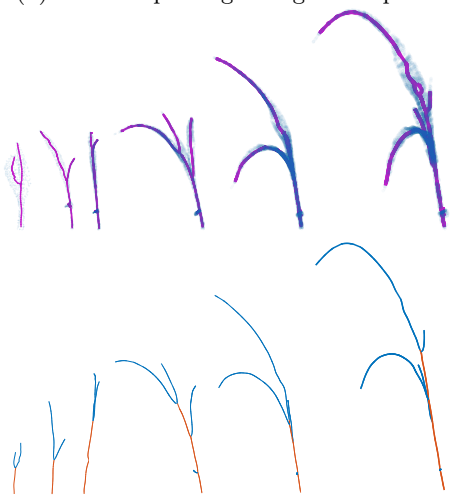

(c) Another example of a growing maize plant.

Fig. 1: Examples of 4D plants from the Pheno4D dataset. For each example, we show the original point cloud with the computed 3D skeleton overlayed on it (first row), and the decomposition of the 3D skeleton into layers (second row). The red branch is the main branch, blue corresponds to the 2^{nd} layer of branches, yellow to the 3^{rd} layer, and purple to the 4^{th} layer.

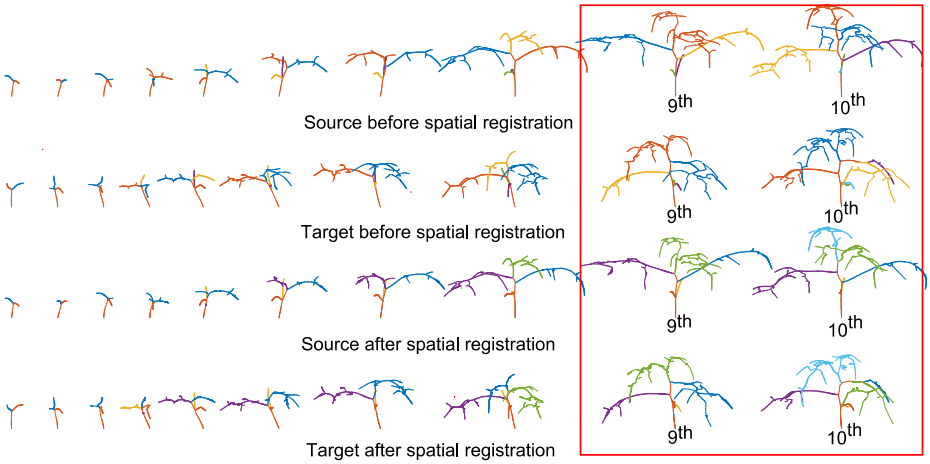

Fig. 2: Example of spatial registration of 3D tree-shaped structures within and across 4D trees. The colors indicate branch-wise correspondences before (1st and 2nd rows) and after (3rd and 4th rows) spatial registration. We only show correspondences up to the second level of the tree hierarchy. Figs. 3 and 4 provide a close zoom-in on the highlighted trees.

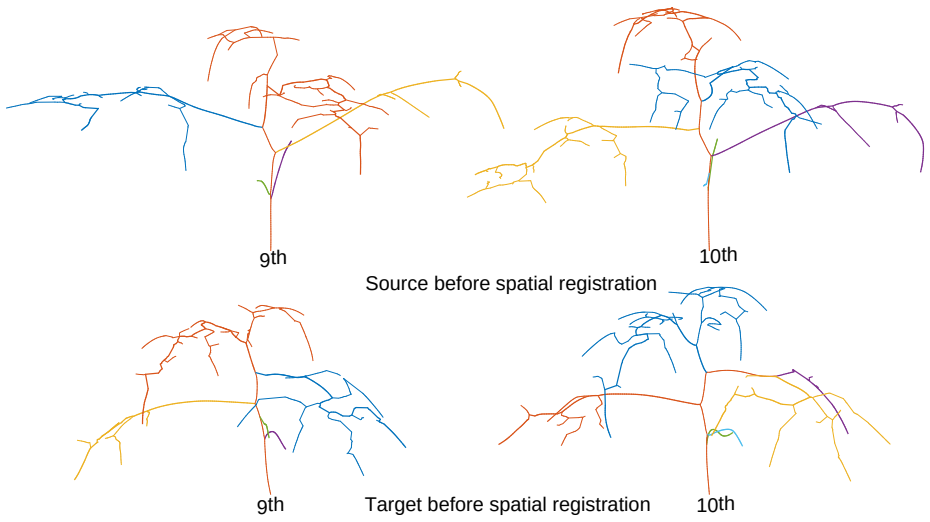

(a) Before spatial registration.

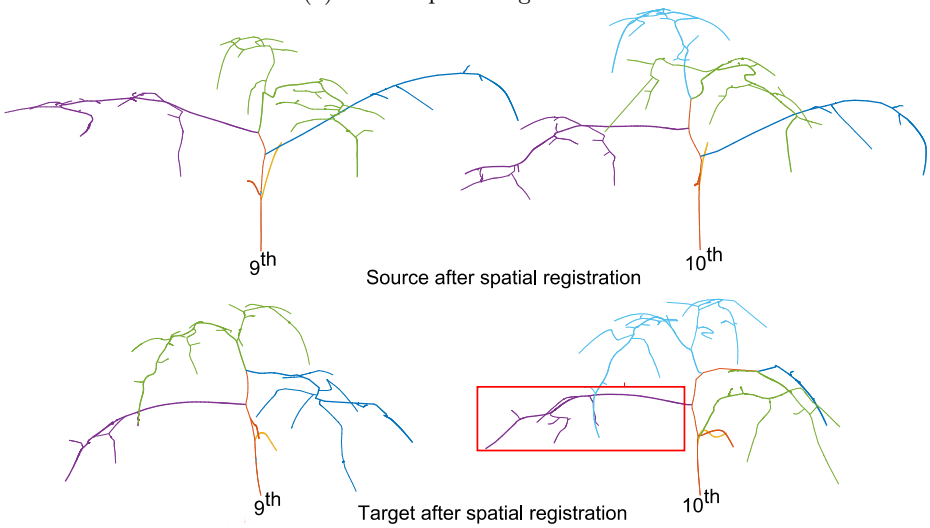

(b) After spatial registration.

Fig. 3: A zoom-in on the the 9th and 10th trees of Fig. 2, before and after spatial registration. The correspondences are shown up to the second layer. Fig. 4 provides a zoom-in on the correspondences at the third layer of the tree section highlighted with a red box.

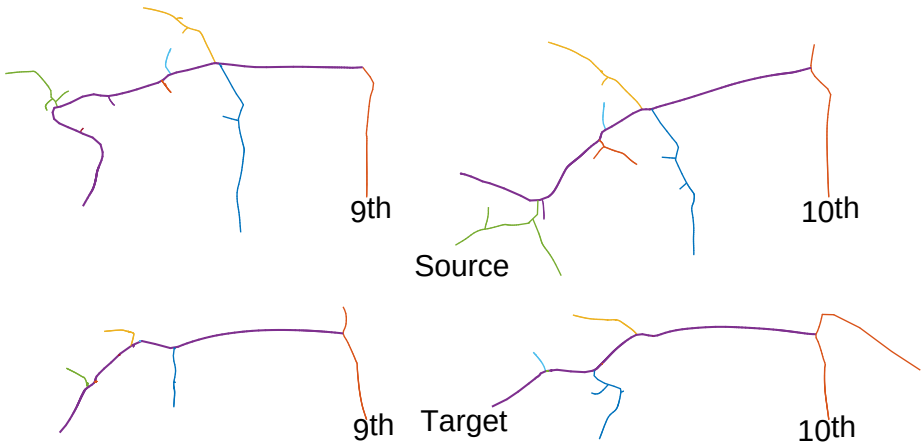

Fig. 4: Illustration of the branchwise correspondences at the third layer of the 4D tree-shaped structures of Figs. 2 and 3. The correspondences are shown for the region highlighted with a red box in Fig. 3.

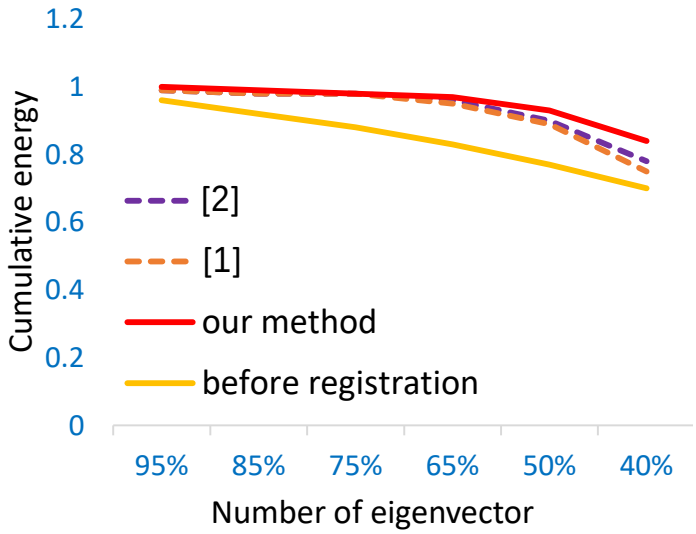

Fig. 5: The cumulative energy as a function of the no. of eigenvectors. Previous methods exhibit a high loss of energy when using less than 65% of the eigenvectors.

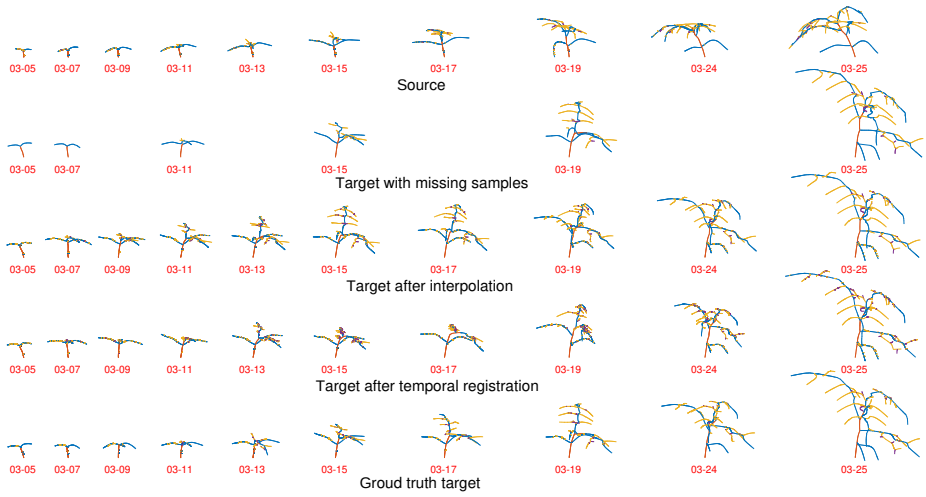

Fig. 6: An example of the temporal registration of 4D tomato plants. The numbers below each tree are the dates, in MM-DD format, when each sample is captured.

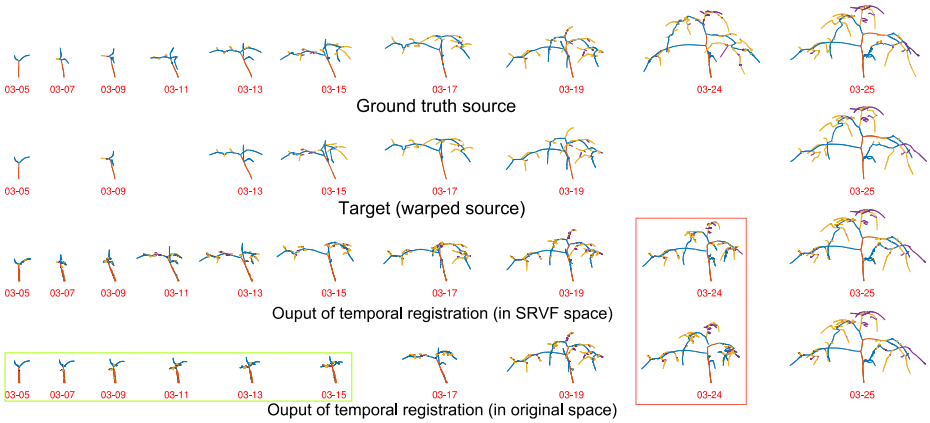

(a) temporal registration in the SRVF space (third row) and the original space (fourth row) of the source (top row) and the target (second row). The green box highlights some incorrect temporal registration that happens in the original space. 7b and Figure 7c provide a zoom-in on the region highlighted with a red box.

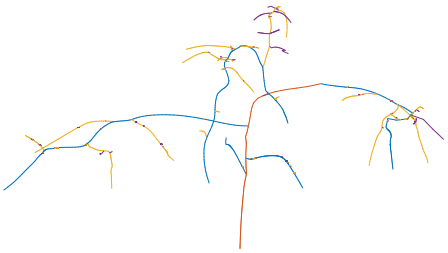

(b) The zoom-in view of a 3D plant from the 4D target temporally registered in SRVF space (top one in the red box of Figure 7a This plant exhibits no bifurcation points separation.

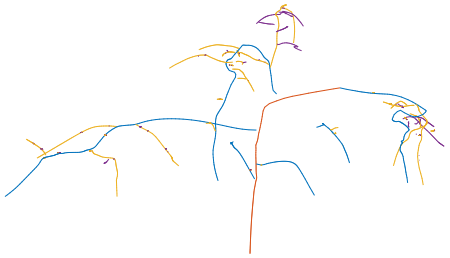

(c) The zoom-in view of a 3D plant from the 4D target temporally registered in the original space (bottom one in the red box of Figure 7a). This plant exhibits bifurcation points separation.

Fig. 7: Significance of the SRVF representation for the temporal registration.

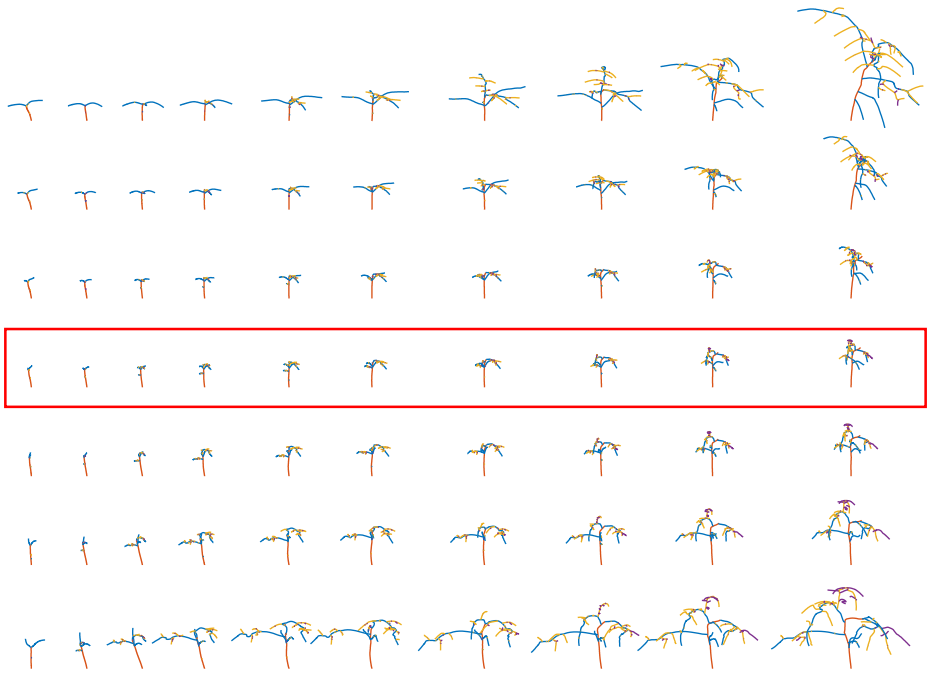

Fig. 8: Example of a 4D geodesic path, before spatiotemporal registration, computed between a 4D tree shape (top row) and a target 4D tree shape (bottom row). The highlighted middle row corresponds to the mean of the source and target 4D plants.

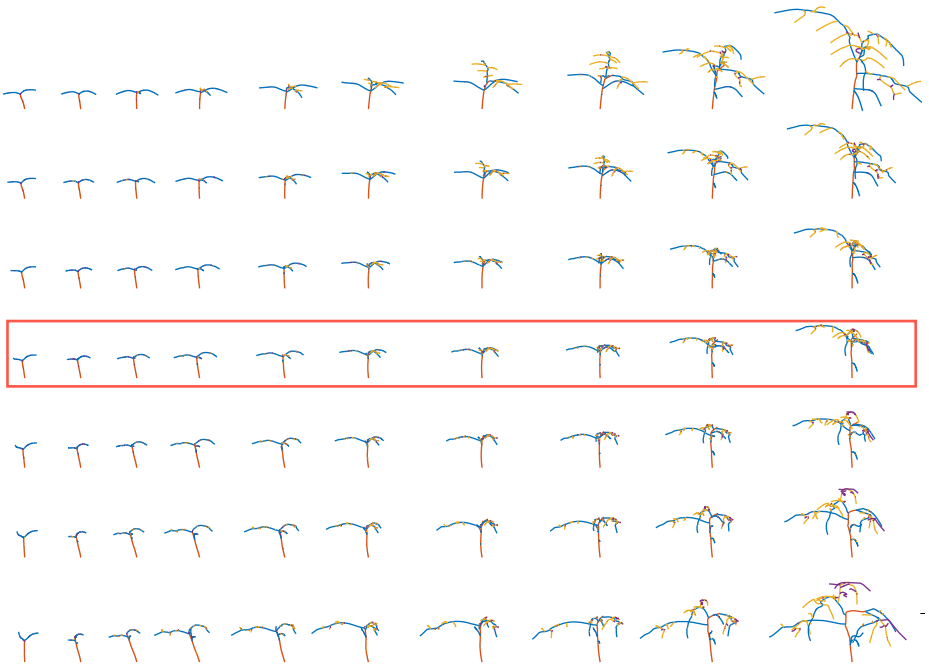

Fig. 9: Example of a 4D geodesic path between the two 4D tree shapes of Fig. 8 but this time after performing spatiotemporal registration. The top row corresponds to the source, while the bottom row corresponds to the target. The middle row, highlighted with a red rectangle, corresponds to the mean of the source and the target 4D plants.

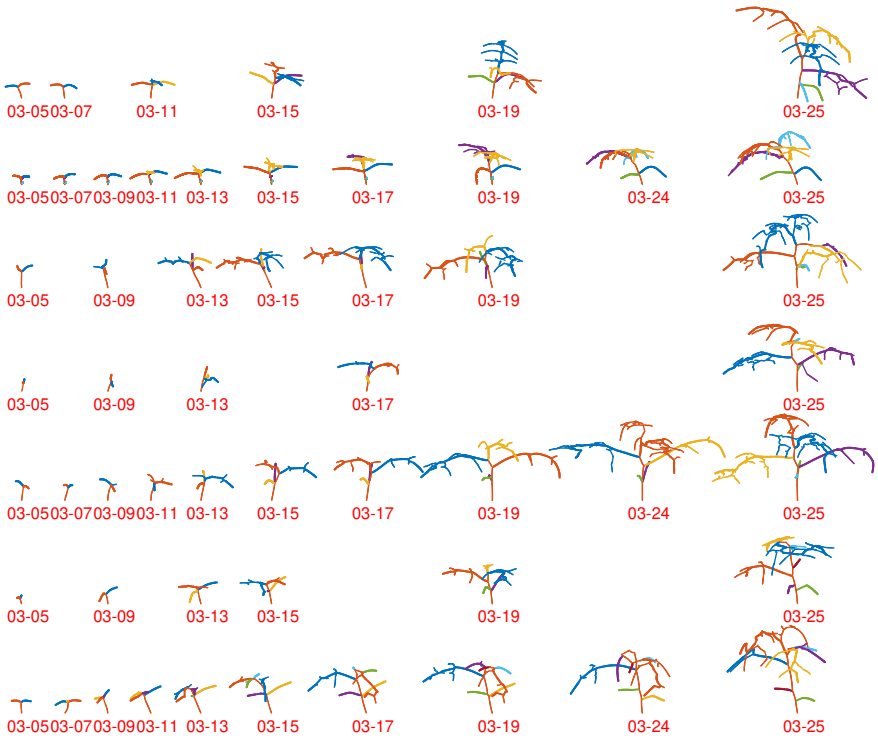

(a) Seven unregistered 4D tomato plants (one per row). The number under each plant indicates the capture date, written in MM-DD format.

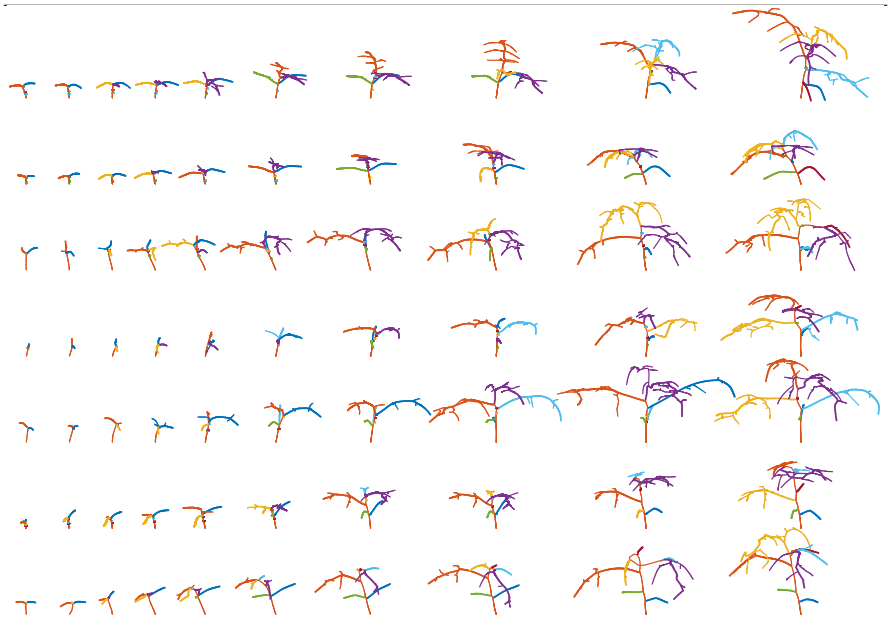

(b) The seven 4D plants (one per row) after their co-registration.

Fig. 10: Seven 4D tomato plants from Pheno4D dataset before and after their spatiotemporal registration. Color codes represent the branch-wise correspondences.

Fig. 11: The mean 4D plant shape of the seven registered 4D tomato plants in Fig. 10b.

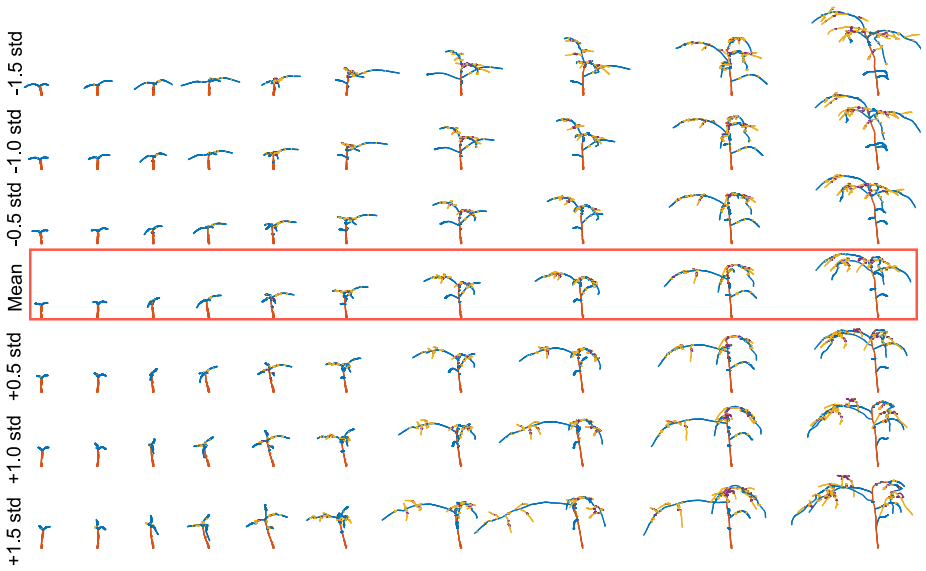

(a) First mode of variation.

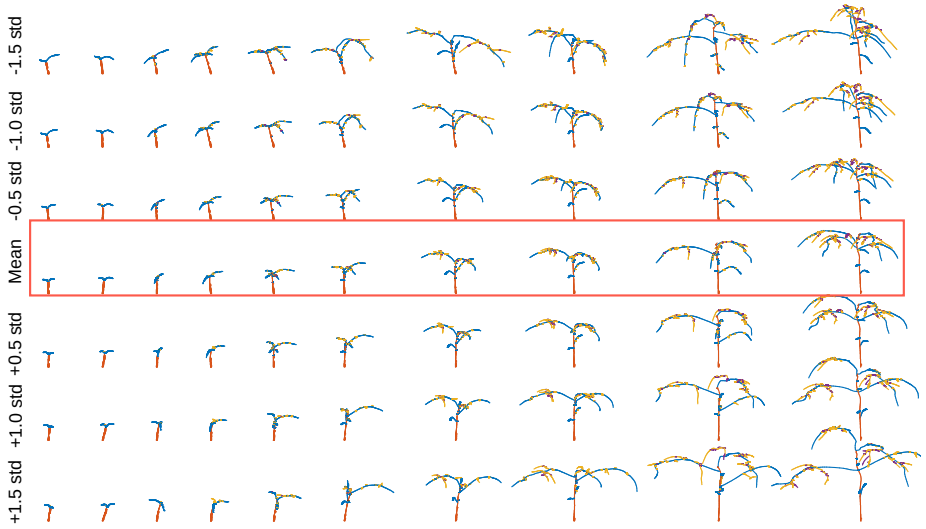

(b) Second mode of variation.

Fig. 12: First **(a)** and second **(b)** principal directions of variation. Each row corresponds to one 4D plant sampled between -1.5 to 1.5 times the standard deviation along the principal direction of variation. The mean 4D plant is highlighted in red.

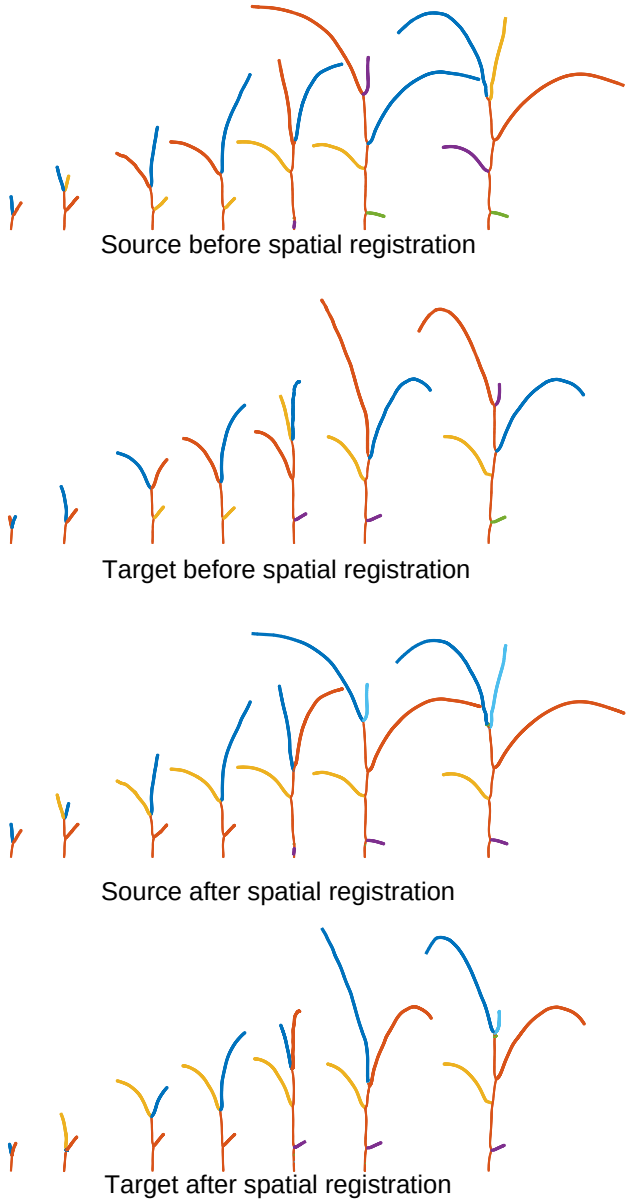

Fig. 13: Example of spatial registration of two 4D tree-shaped structures (of maize plants). Colors indicate branch-wise correspondences before (1st and 2nd rows) and after (3rd and 4th rows) spatial registration.

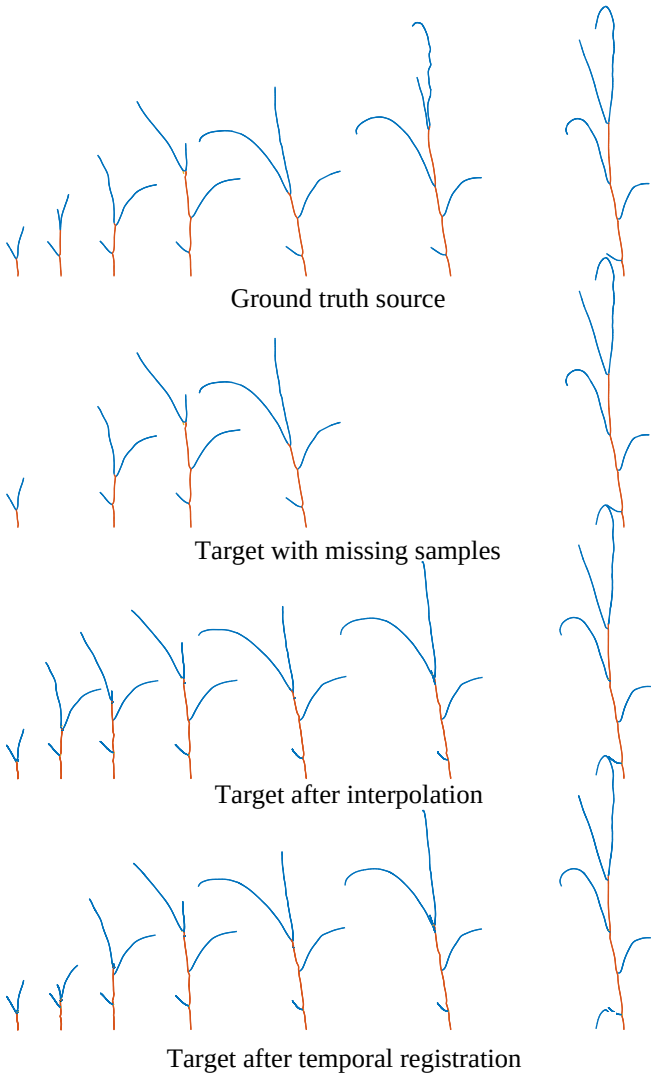

Fig. 14: An example of the temporal registration of 4D maize plants.

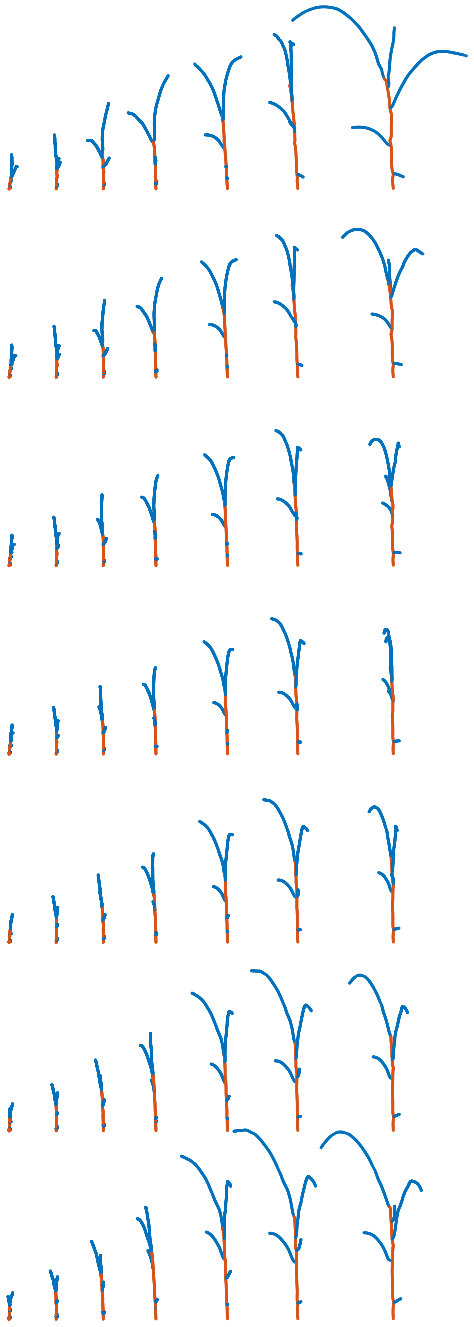

Fig. 15: The 4D geodesic between two 4D maize tree shapes before spatiotemporal registration. The top row corresponds to the source and the bottom row corresponds to the target.

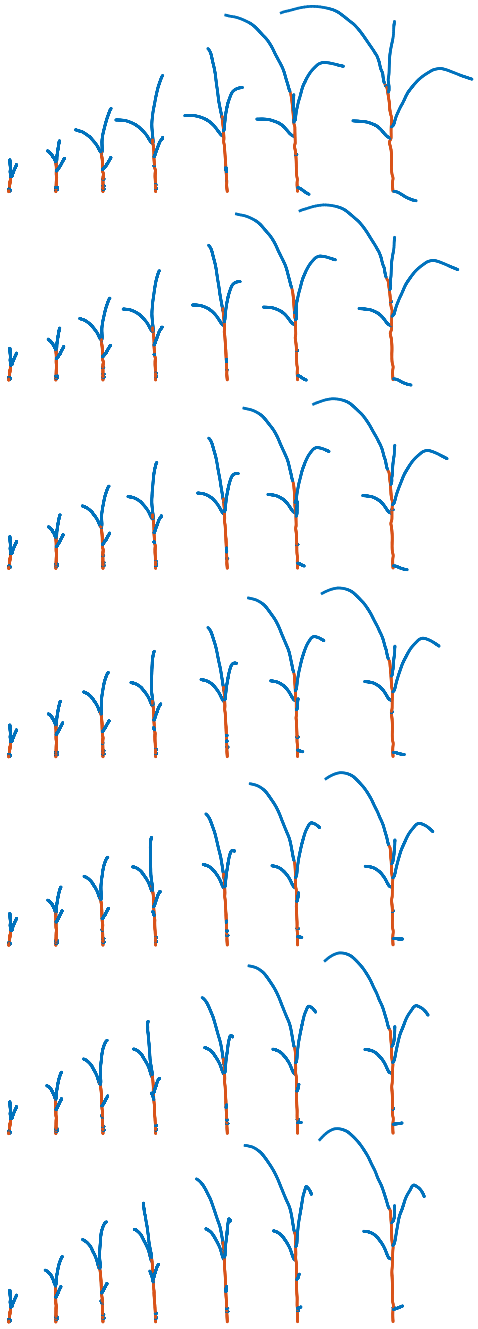

Fig. 16: The 4D geodesic between the two 4D maize tree shapes of Fig. 15 after spatiotemporal registration. The top row corresponds to the source and the bottom row corresponds to the target.

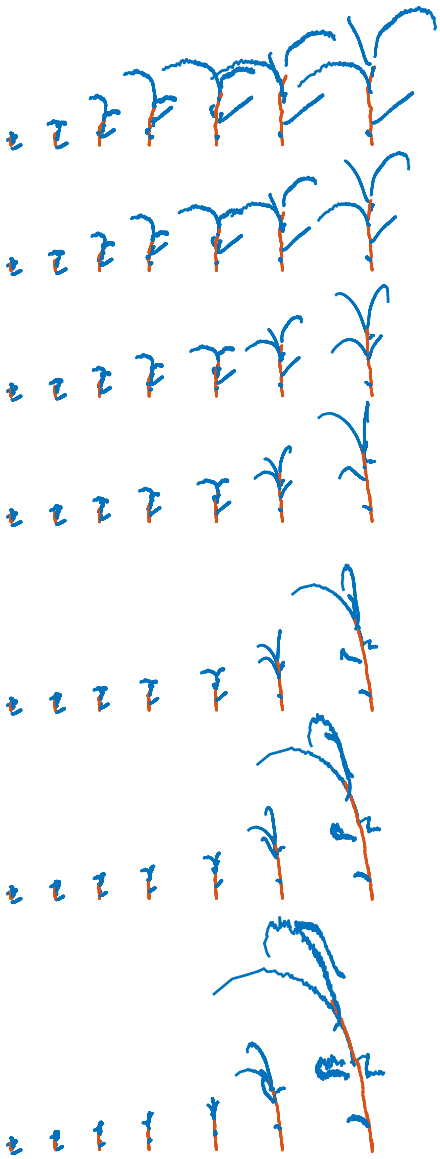

Fig. 17: The 4D geodesic between two 4D maize tree shapes (same 4D shapes of Figs. 15 and 16) calculated in the original tree shape space. The top row corresponds to the source and the bottom row corresponds to the target. Since we compute the geodesic in the original space (not the SRVFT space of trees) we notice a significant noise in the output.

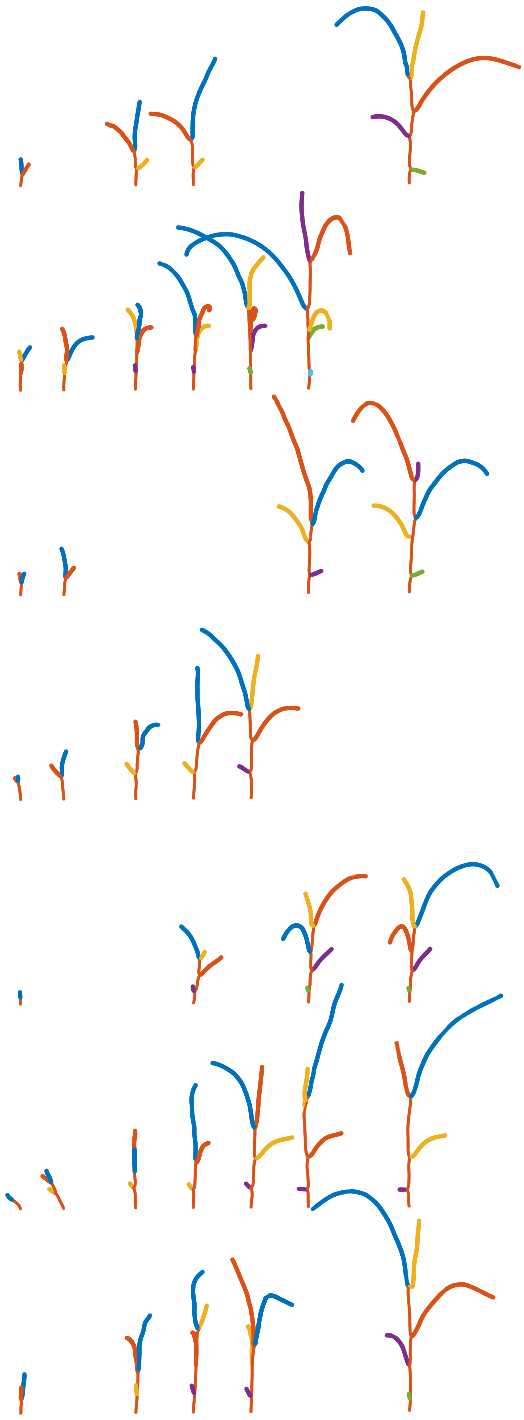

Fig. 18: Seven unregistered 4D maize plants. Each row corresponds to a 4D plant. The colors indicate the correspondence between trees.

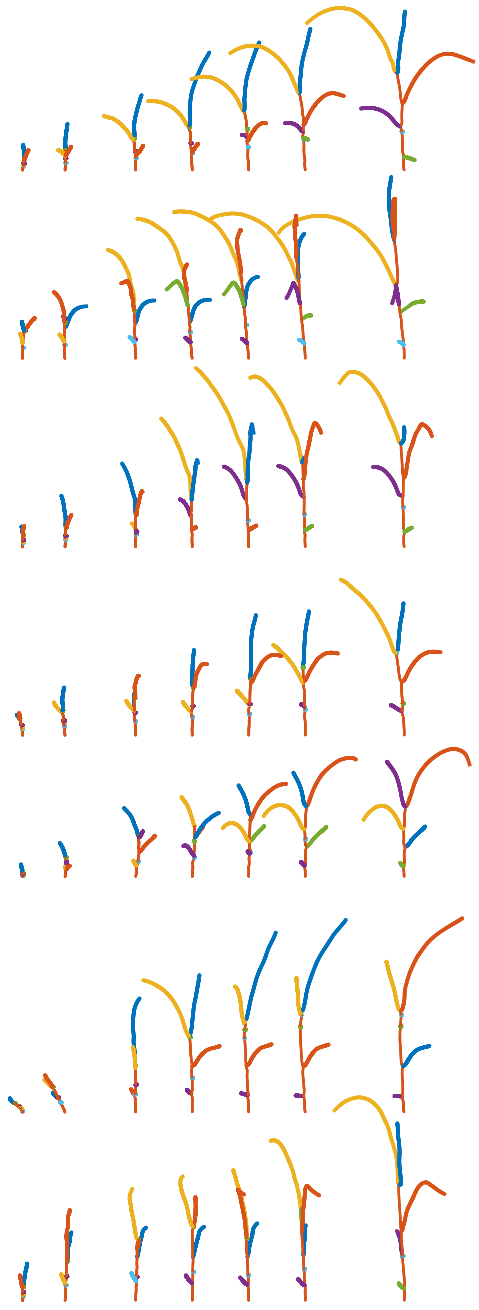

Fig. 19: The co-registered seven 4D maize plants. Each row corresponds to the 4D plants of the same row in Fig. 18. The colors indicate the correspondence between trees.

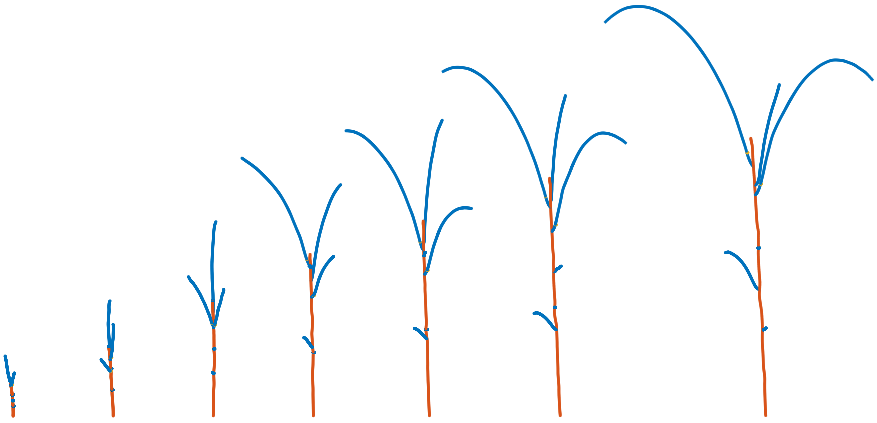

Fig. 20: The mean 4D plant shape of the seven registered 4D maize plants in Fig. 19.

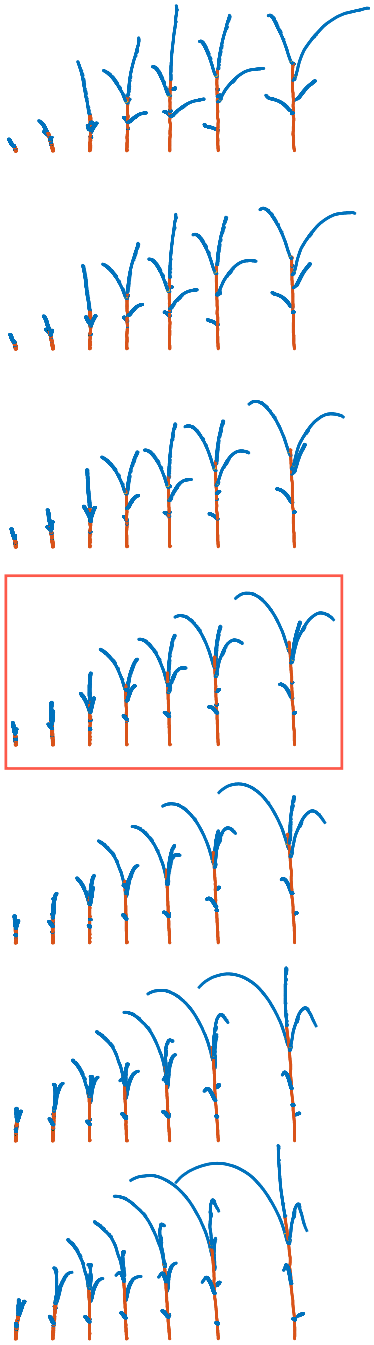

Fig. 21: First principal directions of variation of the set of maize plants in Fig. 19. Each row corresponds to one 4D plant sampled between -1.5 to 1.5 times the standard deviation along the principal direction of variation. The mean 4D plant is highlighted in red.

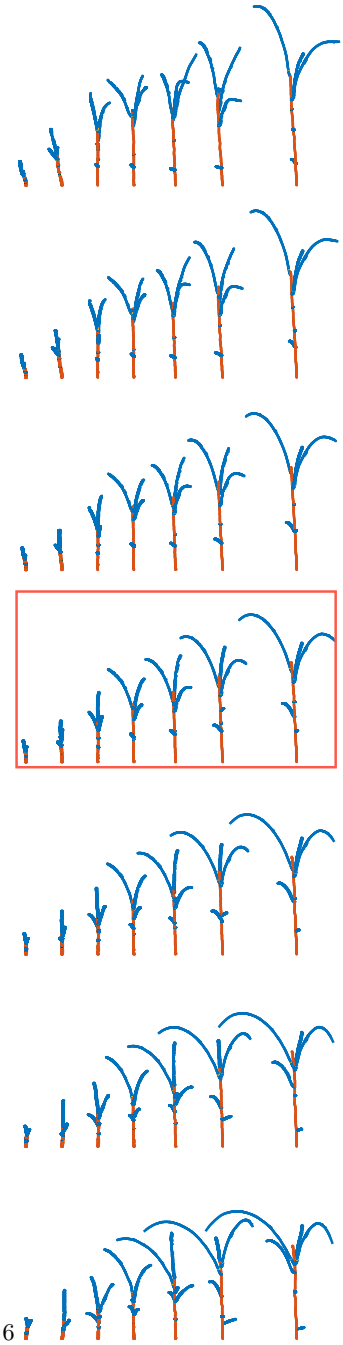

Fig. 22: Second principal directions of variation of the set of maize plants in Fig. 19. Each row corresponds to one 4D plant sampled between −1.5 to 1.5 times the standard deviation along the principal direction of variation. The mean 4D plant is highlighted in red.

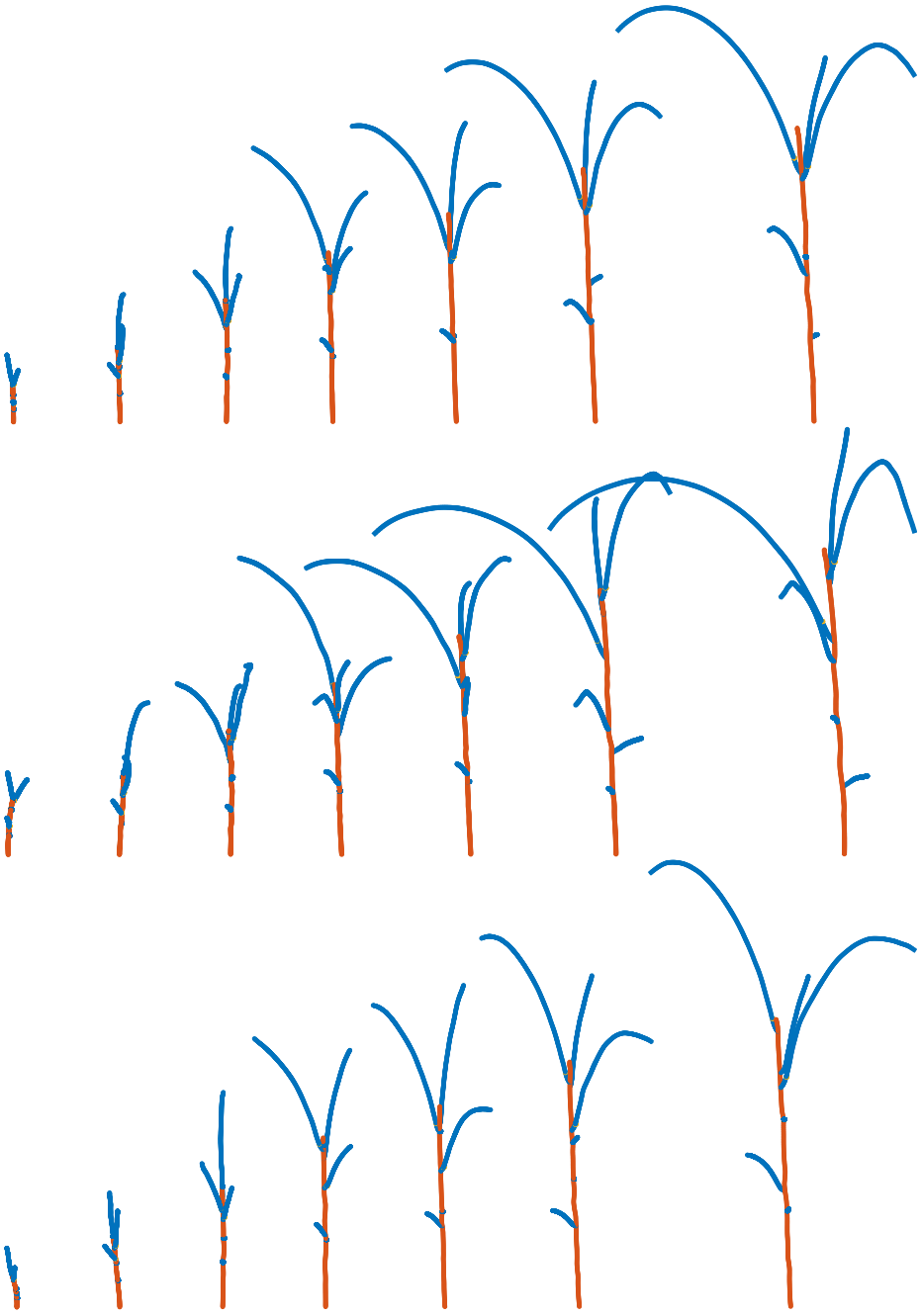

Fig. 23: Three randomly synthesized 4D maize plants. Each row corresponds to a random 4D plant.

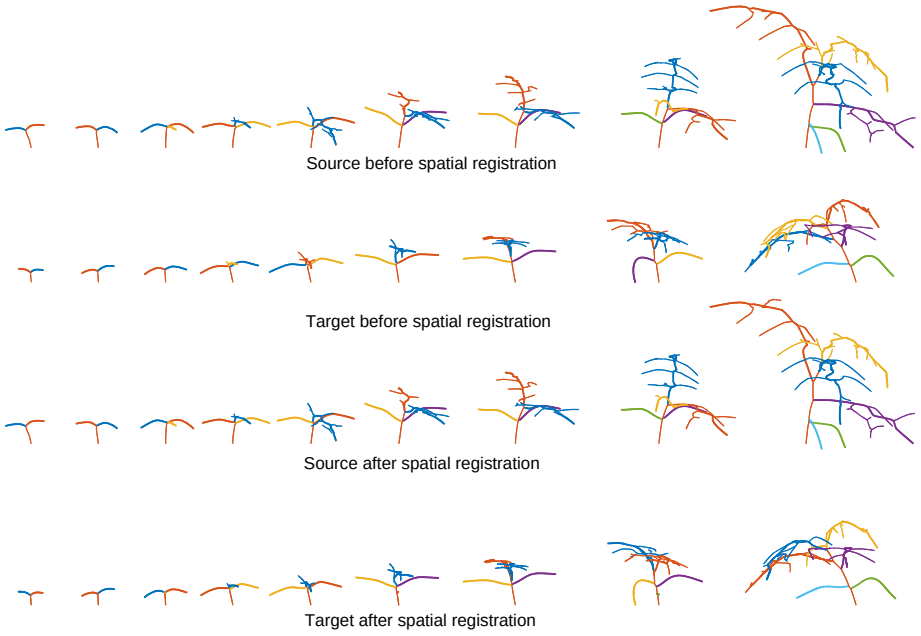

Fig. 24: An Example of spatial registration of 3D tree-shaped structures across two 4D tomato trees. The colors indicate branch-wise correspondences before (1st and 2nd rows) and after (3rd and 4th rows) spatial registration. We only show correspondences up to the second level of the tree hierarchy.

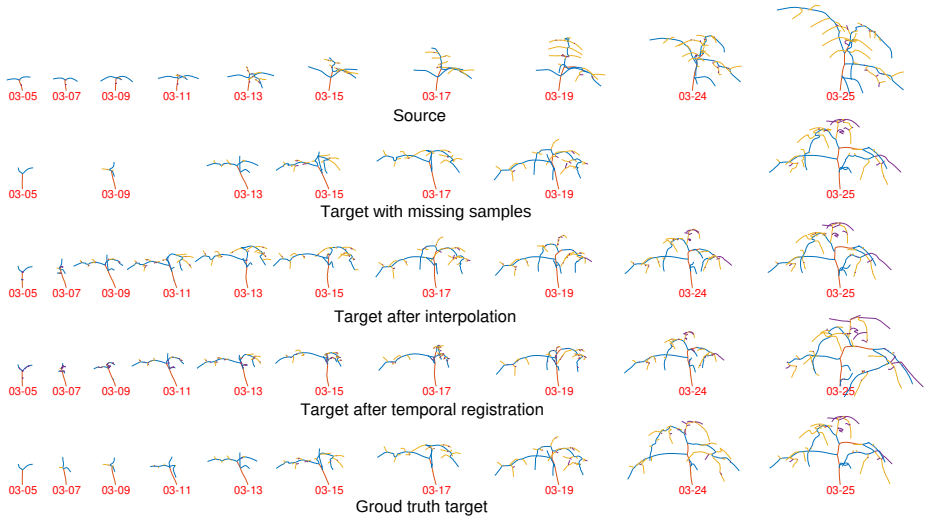

Fig. 25: An example of the temporal registration of 4D tomato plants. The numbers below each tree are the dates, in MM-DD format, when each sample is captured.

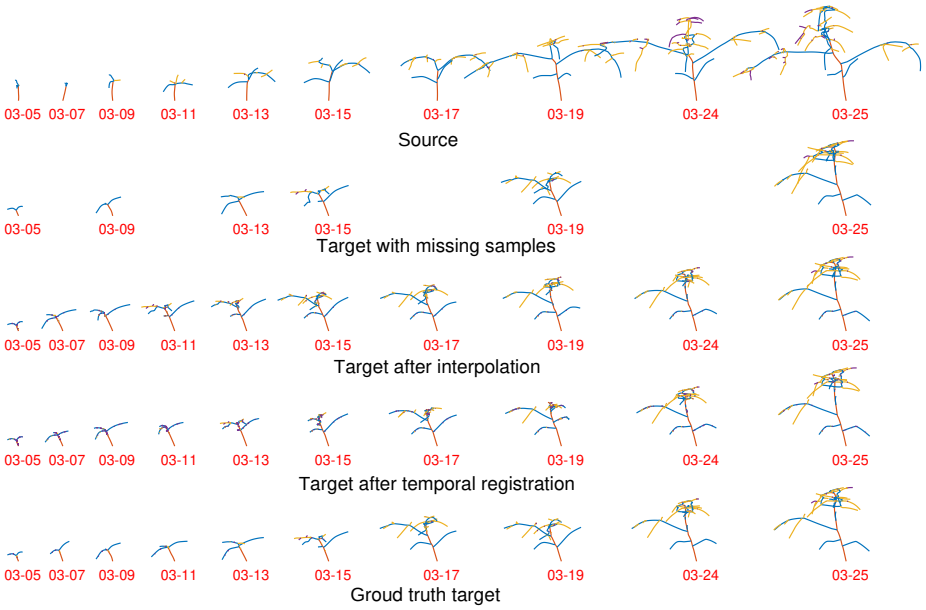

Fig. 26: Another example of the temporal registration of 4D tomato plants. The numbers below each tree are the dates, in MM-DD format, when each sample is captured.

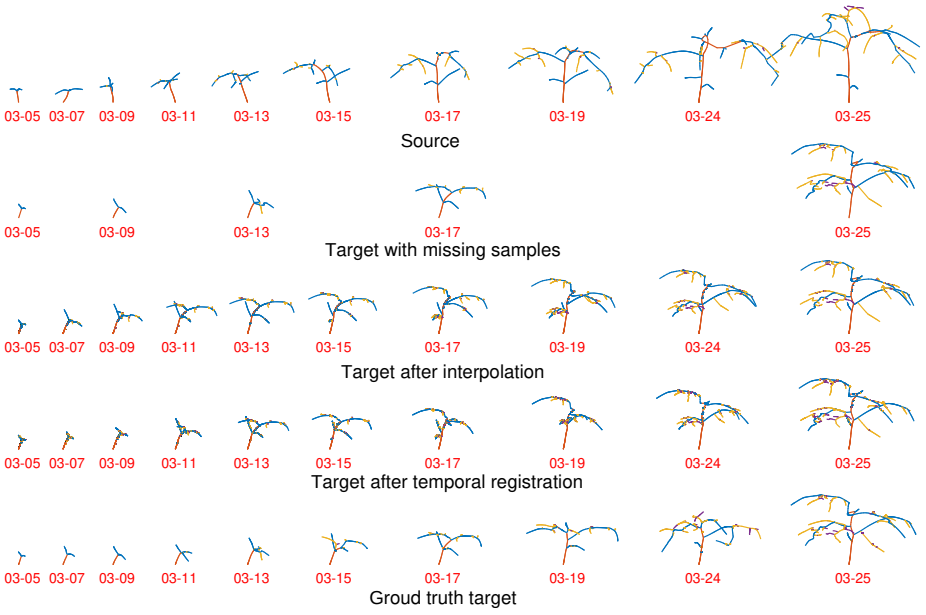

Fig. 27: Another example of the temporal registration of 4D tomato plants. The numbers below each tree are the dates, in MM-DD format, when each sample is captured.

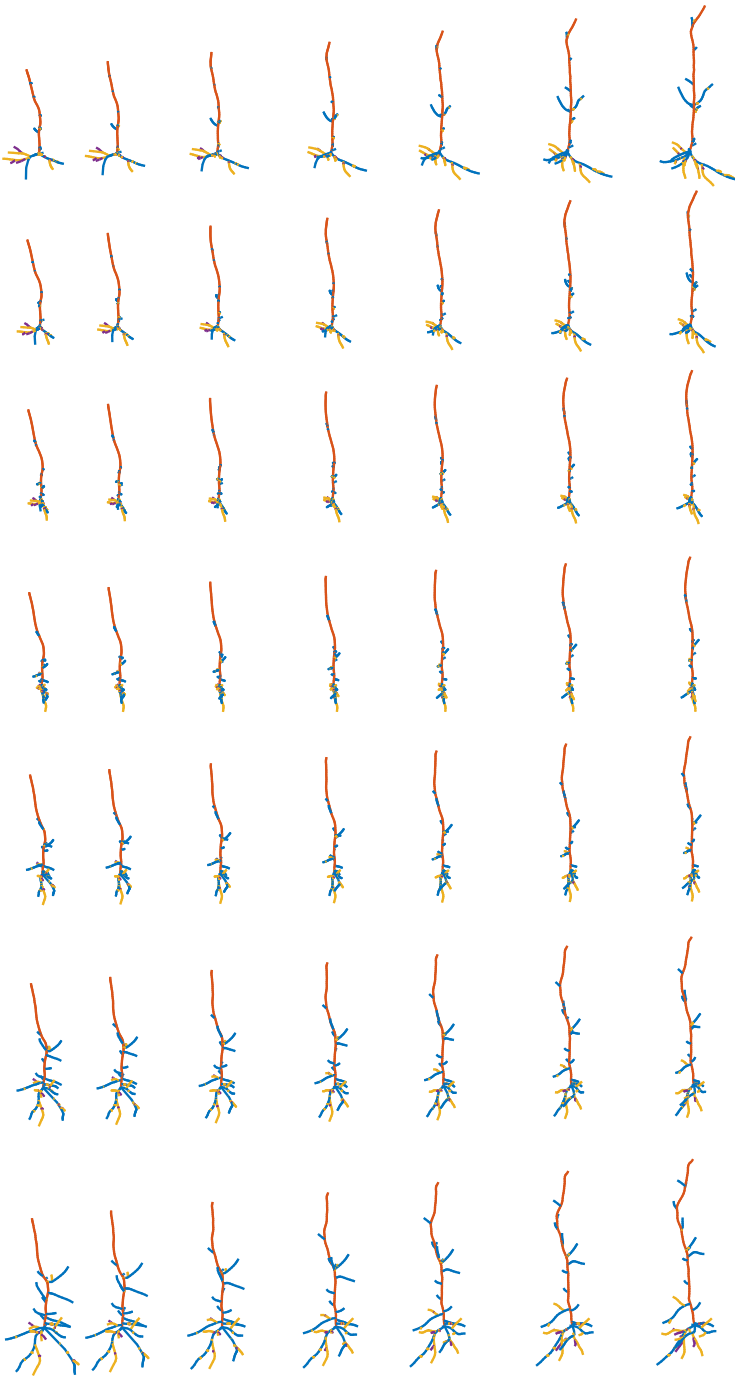

Fig. 28: Example of a 4D geodesic path, before spatiotemporal registration, computed between a simulated 4D neuron shape (top row) and a simulated target 4D tree shape (bottom row). The highlighted middle row corresponds to the mean of the source and target 4D neurons.

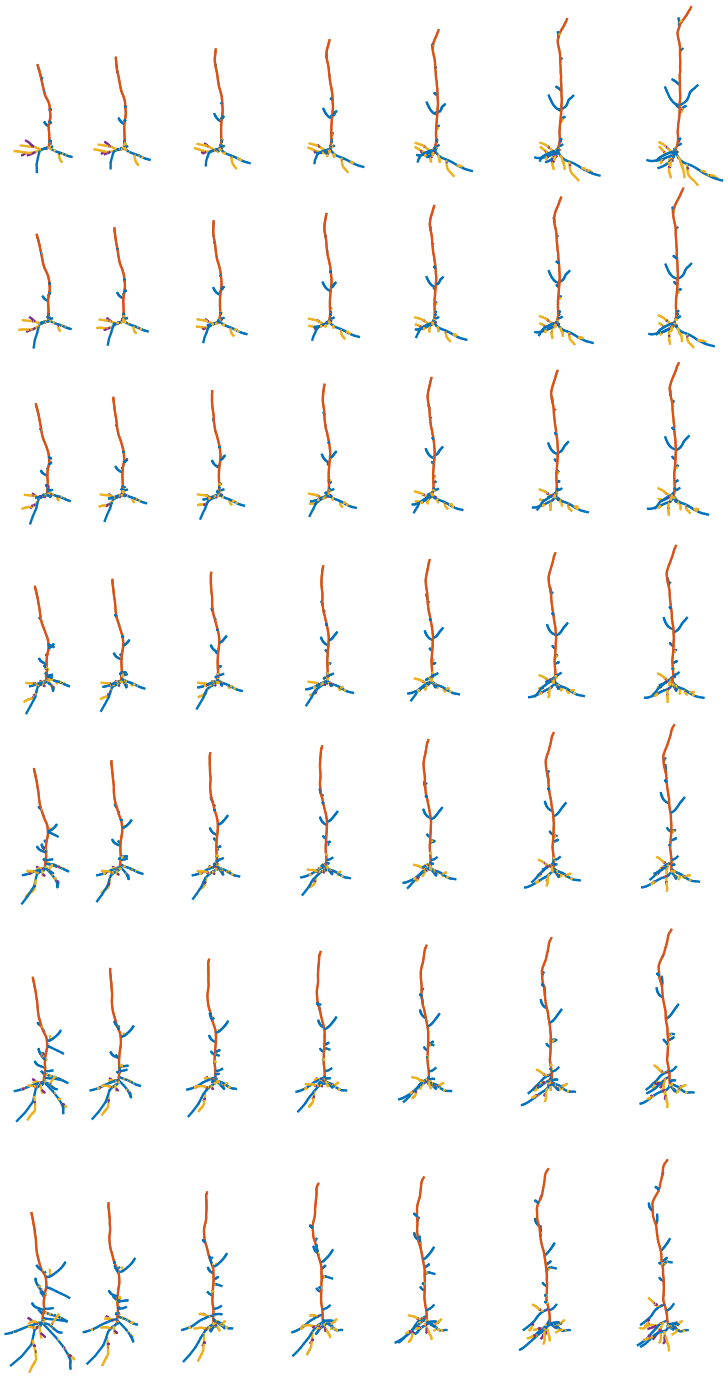

Fig. 29: Example of a 4D geodesic path between the two simulated 4D neuron shapes of Fig. 28 but this time after performing spatiotemporal registration. The top row corresponds to the source, while the bottom row corresponds to the target. The middle row, highlighted with a red rectangle, corresponds to the mean of the source and the target 4D neurons.